Observing the Structures of Protoplanetary Disks

Sean M. Andrews

Center for Astrophysics | Harvard & Smithsonian
Cambridge, Massachusetts, USA 02138; email: sandrews@cfa.harvard.edu

Annu. Rev. Astron. Astrophys. 2020. 58:1–18

https://doi.org/10.1146/((please add article doi))

Keywords

keywords, separated by comma, no full stop, lowercase

Abstract

Debris disks are tenuous, dust-dominated disks commonly observed around stars over a wide range of ages. Those around main sequence stars are analogous to the Solar System's Kuiper Belt and zodiacal light. The dust in debris disks is believed to be continuously regenerated, originating primarily with collisions of planetesimals. Observations of debris disks provide insight into the evolution of planetary systems; and the composition of dust, comets, and planetesimals outside the Solar System; as well as placing constraints on the orbital architecture and potentially the masses of exoplanets that are not otherwise detectable. This review highlights recent advances in multiwavelength, high-resolution scattered light and thermal imaging that have revealed a complex and intricate diversity of structures in debris disks and discusses how modeling methods are evolving with the breadth and depth of the available observations. Two rapidly advancing subfields highlighted in this review include observations of atomic and molecular gas around main sequence stars and variations in emission from debris disks on very short (days to years) timescales, providing evidence of non-steady-state collisional evolution particularly in young debris disks.

- First finding.
- Second finding.
- Third finding.

Contents

1. INTRODUCTION

1.1. Motivation

The formation and early evolution of a star and its planets are fundamentally governed by their relationships with a circumstellar disk. The telltale signatures of the foundational interactions between disk, star, and planets are imprinted on the disk structure – the detailed spatial distribution and physical conditions of the disk material. Measurements of disk structures, complemented with theoretical simulations, can be used to figure out how the key physical mechanisms associated with star and planet formation operate.

Star formation begins with the gravitational collapse of an over-density (core) in a molecular cloud. Rotation of that core implies that material from its outer regions, with higher angular momentum, is channeled onto a flattened disk that orbits a central protostar, rather than directly onto the star itself (Cassen & Moosman 1981, Terebey et al. 1984). In that sense, disks are a simple consequence of angular momentum conservation. Measurements of young disk structures, still embedded in their natal core material (envelope), reveal much about the star formation process: their sizes help distinguish the roles that magnetic fields have in regulating core collapse; their masses constrain the typical protostellar accretion

rates; and their density distributions encode the mechanics of angular momentum transfer and accretion that ultimately determine the stellar mass.

Disks are also the birthplaces of planetary systems. The prevalence, formation modes, masses, orbital architectures, and compositions of planets depend intimately on the physical conditions in the disk at their formation sites, the evolution of that disk structure (locally and globally), and the planetary migration driven by dynamical interactions with the disk material. Measurements of the disk mass and its spatial distribution offer crucial boundary conditions for models of planet formation. Combined with the demographic properties observed in the mature exoplanet population, that information can help develop and refine a predictive formation theory, despite the considerable complexity of the associated physical processes (e.g., Ida & Lin 2004, Alibert et al. 2005).

1.2. Observational Primer

In many ways, disk structures offer profound insights on how the properties of stars and planetary systems are shaped by their origins. This review is focused on the recent landscape of observational constraints on disk structures: how relevant measurements are made, what they suggest about disk properties, and how those properties are connected to star and planet formation. The key measurements of disk structures require high angular resolution data, as the typical disk in a nearby star-forming region subtends only $\sim 1''$ on the sky. Most of any given disk is relatively cool enough (temperatures $<$100 K) that it emits most efficiently in the millimeter-wave part of the spectrum (hereafter mm, meaning $\lambda \approx 0.5$–5 mm). Coupling these small angular sizes and cool temperatures, considerable emphasis in this review will be placed on radio interferometry as an essential tool. Indeed, dramatic progress over the past decade has largely been driven by the commissioning of the transformational Atacama Large Millimeter/submillimeter Array (ALMA) facility.

sub-mm: $\lambda \approx 0.1$–0.5 mm, $\nu \approx 0.6$–3 THz.

mm: $\lambda \approx 0.5$–5 mm, $\nu \approx 60$–600 GHz.

cm: $\lambda \approx 5$–50 mm, $\nu \approx 6$–60 GHz.

Three categories of observational tracer are useful for studying disk structures: scattered light, thermal continuum emission, and (primarily molecular) spectral line emission. The first two are sensitive to the physical conditions and distribution of solids, and the third is used to measure the properties of the gas. Each observational probe is sensitive to different materials and physical conditions, ensuring considerable diversity in the disk appearance when viewed in different tracers. An illustrative example is shown in **Figure ??**.

1.2.1. Scattered Light. Small (μm-sized) dust grains suspended in the disk atmosphere can reflect the optical and infrared radiation emitted by the the central host star. This scattered light is especially sensitive to the vertical distribution of the dust, and how it changes with radius (e.g., Debes et al. 2013, Stolker et al. 2016, Garufi et al. 2017). Spectral and polarization variations in the scattered light morphology can constrain the albedo and phase function of the scatterers, which are set by the size, shape, and composition of the grains (Debes et al. 2008, Min et al. 2012, 2016). Aside from uniquely probing the dust disk surface geometry, the key advantage of this tracer is resolution: adaptive optics systems operating at the diffraction limit on 8–10 m telescopes measure features at 30–50 mas scales ($\sim$5 au). The important challenges are contrast with the host stars, which prevent measurements in the innermost disk ($\lesssim$ 10 au), and sensitivity at large radii, due to the dilution of the stellar radiation field. The latter issue has limited the sample of resolved scattered light measurements, and biased it toward disks with brighter (earlier type) hosts.

1.2.2. Continuum Emission. Disk solids also emit their own thermal continuum radiation that spans at least four decades in wavelength (from 1 μm to 1 cm). Most of that emission is optically thick, and therefore a diagnostic of the temperature structure in the disk (e.g., see Andrews 2015). Lower optical depths (τ_ν) are available at longer wavelengths, with the transition to optically thin traditionally expected in the sub-mm. In the optically thin limit ($\tau_\nu \ll 1$), the continuum intensities scale with the product $I_\nu \propto \kappa_\nu B_\nu(T)\Sigma_s$, where κ_ν is the opacity (absorption cross section per unit mass), $B_\nu(T)$ the Planck function at the local temperature T, and Σ_s the surface density of solids. The mm continuum spectrum has a roughly power-law shape, $I_\nu \propto \nu^{\alpha_{\rm mm}}$, with the spectral index set by the sum of contributions from the Planck function ($B_\nu \propto \nu^{\alpha_{\rm Pl}}$, where $\alpha_{\rm Pl} \approx 1.7$–$2.0$ for $T > 15$ K) and the opacity spectrum ($\kappa_\nu \propto \nu^\beta$), so $\alpha_{\rm mm} \approx \alpha_{\rm Pl} + \beta$ (Beckwith & Sargent 1991, Ricci et al. 2010b,a). The opacity index, β, depends on the sizes, shapes, and compositions of the solids (Miyake & Nakagawa 1993, D'Alessio et al. 2001, Draine 2006).

In principle, resolved measurements of the mm continuum provide an ideal opportunity to constrain the mass distribution (and particle properties) of the disk solids. This broadband tracer is also relatively easy to observe at high resolution, down to 10–20 mas scales ($\sim$2 au; and no contrast issues with the host), thanks to the sensitivity and resolution of ALMA. This means measurements are plentiful: much of the collective knowledge of resolved disk structures is based on mm continuum data. There are two key ambiguities in interpreting these data. First, some of the emission is likely optically thick, perhaps preferentially in the inner disk (see Beckwith et al. 1990, Andrews & Williams 2005). In that case, the intensities saturate to $B_\nu(T)$ and the spectral index reverts to $\alpha_{\rm Pl}$. Self-scattering could diminish the intensities below $B_\nu(T)$ and permit $\alpha_{\rm mm}$ to vary in the range 1.5–2.5, depending on the frequency dependence of the albedo (Zhu et al. 2019, Liu 2019). And second, our relative ignorance of the microphysical particle properties that set κ_ν – their mineralogical (and ice) compositions (Pollack et al. 1994), sizes (Miyake & Nakagawa 1993), and structures (Henning & Stognienko 1996) – means that links between the emission and physical conditions are intrinsically uncertain, even when optical depths are low.

1.2.3. Spectral Line Emission. The dominant constituent by mass in a disk is cold H_2 gas. But, H_2 lacks a permanent dipole moment and is therefore essentially 'dark': there is no direct probe of the gas mass reservoir. Instead, constraints on the structure of the gas disk rely on spatially and spectrally resolved measurements of trace molecular rotational transitions throughout the (sub-)mm bands. Such emission lines can be optically thick or thin. Like the continuum, optically thick line emission has $I_\nu \propto B_\nu(T)$ (where T is formally the excitation temperature, equivalent to the gas temperature in local thermodynamic equilibrium): the key difference is that the line photosphere (where $\tau_\nu \sim 1$) can be located at a higher altitude above the midplane than the continuum (Beckwith & Sargent 1993). For low optical depths, the line intensity scales with the product of the abundance of molecules of that species, the surface density of the gas, and the temperature, $I_\nu \propto [{\rm X}/{\rm H_2}]\Sigma_g B_\nu(T)$. In either case, the spatio-kinematic morphology of the line emission is set by the gas dynamics, dominated by Keplerian rotation around the host star (Marsh & Mahoney 1992, Koerner et al. 1993). The line width is determined by thermal and non-thermal broadening contributions; the latter is typically associated with turbulence (Hughes et al. 2011).

Resolved measurements of multiple optically thick lines with a range of critical densities can be used to trace the temperature structure of the disk atmosphere (e.g., Dartois et al. 2003), and optically thin lines can theoretically be used to constrain gas densities. With

sufficient spectral resolution, such emission line datasets can be used to tomographically reconstruct the disk velocity field (Simon et al. 2000, Rosenfeld et al. 2013a) and assess the level of turbulence (Guilloteau et al. 2012, Flaherty et al. 2015). ALMA is in principle capable of resolving such line emission at tens of milliarcsecond scales (∼2–5 au) in few m s^{-1}-wide velocity channels, but the narrow bandwidths and relatively low abundances of trace molecular species mean that sensitivity is a perennial challenge (particularly when optical depths are low). Accordingly, line measurements of disks with the requisite sensitivity and resolution are considerably less common than for the continuum. The two most prominent challenges in interpreting spectral line data are confusion with the emitting layer location (in the typical case where resolution is limited) and the large (potentially orders of magnitude) uncertainties in the molecular abundances (relative to H_2).

1.3. Statement of Scope

This review covers four broad (and in most respects inter-related) topics that currently occupy much of the effort in the disk community: the impetus and techniques for measuring key properties of disk structures, like masses and density distributions (Section 2); the constraints on evolutionary and environmental dependencies based on demographics studies (Section 3); the evidence for (and problems with) the growth and migration of disk solids (Section 4); and the properties and roles of small-scale *substructures* in shaping observables and facilitating planet formation (Section 5). It concludes with a summary (Section 6) and a discussion of some potentially fruitful avenues for future work (Section 7).

2. KEY STRUCTURE PROPERTIES

The spatial distribution of mass – the density structure – is without question the fundamental property of interest for disks. The over-arching conceptual design of the field presumes that disk evolution is basically deterministic, such that a collection of "snapshots" of disk density distributions that span an appropriate range of environmental and evolutionary states could be used to work out the mechanics of key physical processes and thereby refine a predictive model of how disks regulate star and planet formation. This section of the review is focused on the underlying motivations, observational tracers, and lingering ambiguities associated with attempts to measure the mass distributions in disks. Since the density structure is intrinsically tied to the thermal and dynamical state of the disk, constraints on temperatures (Section 2.4) and kinematics (Section 2.5) are also summarized.

2.1. Masses

Most of the emphasis in the field is on the integrated quantity, disk masses, rather than their density distributions. That is mostly a practical limitation, but many of the key techniques and issues can be illustrated well from this coarser perspective. The primary interest here is that measurements of disk masses offer elementary constraints on the contents of planetary systems. Summing the terrestrial planet and giant planet core masses offers a conservative lower bound on the solid mass of the Solar Nebula disk ($M_s > 45 M_\oplus$; Weidenschilling 1977) or its exoplanet counterparts (e.g., Chiang & Laughlin 2013). Extrapolations of the current planetary atmosphere contents to the primordial H,He-rich gas expected in disks (e.g., Kusaka et al. 1970) enable an analogous limit for the gas masses ($M_g > 0.01 M_\odot$; e.g., Hayashi 1981). The current census of exoplanets finds an abundance of worlds orbiting

Notation, Conventions, and Nomenclature

To set the practical framework for interpreting the results in this field, some discussion of standards and terminology is helpful. The common characterization of the density structure in disks essentially condenses to a one-dimensional description through the radial surface density profil e, Σ, defined such that the mass $M = 2\pi \int \Sigma\, r\, dr$. This is not intended to diminish the azimuthal or vertical dimensions (with coordinates φ and z, respectively), but rather reflects both a convenient simplification and the fact that disks are by their nature geometrically thin. Because of their different physical and observable behaviors, it is also useful to differentiate the disk contents into two broad categories, solids and gas; their density profiles are related by the (vertically averaged) solids-to-gas ratio, $\zeta = \Sigma_s/\Sigma_g$. The goals of this section are to motivate the physical interest in Σ_s and Σ_g, establish the related observable properties, summarize the state of measurements, review some important limitations, and outline the links to the thermal and dynamical structures of disks.

other stars (Howard et al. 2010, Dressing & Charbonneau 2013), but the efficiency of the metamorphosis of disk material into planetary systems is unclear without a comparison of the mass reservoirs in the parent and descendent populations.

2.1.1. Observational Tracers. Disk solids are a minor contributor to the total mass (∼1%), but the crucial roles they play in all aspects of disk evolution and planet formation justify special attention to their mass reservoir, M_s. Solids emit a broadband thermal continuum spectrum that depends on their temperature and microphysical properties (composition, internal structure, size). Assuming reasonable properties for the solids and disk physical conditions, optical depths have traditionally been expected to be low enough at microwave wavelengths that the continuum luminosity is proportional to M_s (Beckwith et al. 1990).

microwave: Generic term adopted here to refer to wavelengths from a few hundred μm to a few cm.

Of course, the continuum spectrum emitted by solids in a typical disk spans at least four decades in wavelength (∼1 μm to 1 cm). But most of it is optically thick, and therefore more a diagnostic of the thermal structure than the mass. High resolution infrared imaging can also trace scattered starlight from the small solids lofted high above the disk midplane, but again such measurements are insensitive to the mass. While these alternate tracers are unquestionably informative in other contexts, the comparatively bright microwave continuum and its unique access to M_s make it an especially valuable probe.

Most of the mass in a disk is H_2 gas. However, H_2 lacks a permanent dipole moment and is therefore essentially 'dark': there is no *direct* probe of the dominant gas reservoir. Constraints on gas masses in disks (M_g) must instead be derived from the spectral line emission of rarer molecule species. The optimal tracers are optically thin emission lines from molecules that have a reasonably well-understood abundance relative to H_2. In such a case, the emission line luminosity can be converted into a measurement of M_g.

In the literature, two tracer molecule options have been considered for M_g constraints: HD (the primary isotopologue of H_2) and CO. The advantage of HD is the simplicity of its associated chemical network, meaning the HD/H_2 abundance ratio is known well (Bergin et al. 2013, McClure et al. 2016, Trapman et al. 2017). But with a ground state transition in the far-infrared (112 μm), HD measurements are scarce (and currently inaccessible). CO is a popular alternative, but the rotational lines from the primary isotopologue are very optically thick (Beckwith & Sargent 1993). Therefore, gas mass estimates rely on line luminosity

measurements of rarer isotopologues, usually ^{13}CO and C^{18}O together (Williams & Best 2014). The advantages of CO tracers are practical, since these lines are (relatively) bright and accessible (with a sequence of transitions throughout the microwave spectrum), but their abundances are more uncertain. For reference, the utility of a suite of (less favorable) alternative tracers for M_g measurements were explored by Molyarova et al. (2017).

2.1.2. Overview of Mass Measurements. The advent of bolometer detectors on single-dish microwave telescopes motivated a series of continuum photometry surveys designed to measure M_s for hundreds of disks starting 30 years ago (Weintraub et al. 1989, Beckwith et al. 1990, Andre & Montmerle 1994, Osterloh & Beckwith 1995, Andrews & Williams 2005, 2007a), and continuing today with more sensitive interferometers (e.g., Andrews et al. 2013, Ansdell et al. 2016, Cieza et al. 2019). The microwave continuum luminosities (hereafter $L_{\rm mm}$) from these surveys span at least three orders of magnitude. Though this composite $L_{\rm mm}$ distribution is clearly influenced by observational and physical selection effects (see Section 3), it helps provide some rough guidance on M_s values. For some fiducial assumptions for the disk-averaged temperature ($\langle T \rangle \approx 20$ K, based on crude models of infrared emission; Andrews & Williams 2005) and opacity ($\langle \kappa_\nu \rangle \approx 2.3$ cm^2 g^{-1} at $\lambda = 1.3$ mm, as asserted by Beckwith et al. 1990), these luminosities imply a range $M_s \approx 1$–$1000\ M_\oplus$.

There are many fewer available estimates of M_g in disks, owing to the intrinsically more challenging observations of the emission line tracers. The ground state HD emission line was detected from only three disks, suggesting $M_g \geq 0.01 M_\odot$ based on detailed models of their thermal structures (Bergin et al. 2013, McClure et al. 2016). Larger samples of CO isotopologue emission line luminosities typically infer considerably lower values, $M_g < 0.001 M_\odot$ (and detection rates are relatively low; e.g., Ansdell et al. 2016, Long et al. 2017), when referenced to an extensive grid of model structures that assumes the CO/H$_2$ abundance in disks is comparable to the interstellar medium (Williams & Best 2014).

2.1.3. Caveats and Ambiguities. There are large uncertainties in any inference of M_s from microwave continuum data, for two primary reasons. First, the assertion that the emission is optically thin is unlikely to be valid at all disk locations. Once optical depths are high, the emission saturates and mass is hidden (M_s is under-estimated). The significance of this effect depends on the surface area of the thick emission, which will be revisited in various contexts throughout this review. Second, even in the $\tau_\nu \ll 1$ limit, the continuum luminosity scales with the product of the temperature, opacity, and mass. The uncertainty in T will be addressed in Section 2.4. There is considerable ambiguity in M_s estimates due solely to our relative ignorance of the microphysical particle properties that set κ_ν, including their mineralogical (and ice) compositions (Pollack et al. 1994), sizes (Miyake & Nakagawa 1993), and internal structure (porosity; Henning & Stognienko 1996).

Because the particle properties encoded in κ_ν are so fundamentally important for interpreting observations, this latter issue is worth elaboration. The sizes and morphologies of the emitting particles have the most pronounced effects on the behavior of κ_ν. Size distributions are often approximated as power-laws, $n(a) \propto a^{-q}$ for size (radius) $a \in [a_{\rm min}, a_{\rm max}]$, with indices comparable to the expectation for a self-similar collisional cascade ($q \approx 3.5$; Dohnanyi 1969, Tanaka et al. 1996) or more top-heavy variants ($q \approx 2.5$; e.g., Birnstiel et al. 2011). The particle morphologies are characterized by their porosities, usually parameterized with a volume filling factor f_s ($\sim$1 for compact particles, but can be as low as $\sim 10^{-4}$ in aggregates; Kataoka et al. 2013). The microwave opacity spectrum is roughly a

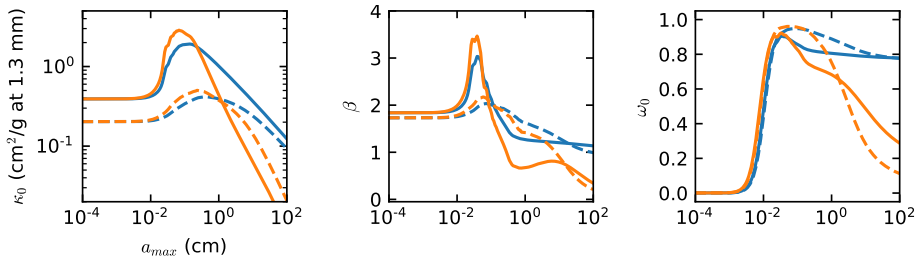

Figure 1

kappa0, beta, albedo as fn of amax (different q, phi, composition, mixing rule, DDA v Mie)

power-law, $\kappa_\nu \approx \kappa_0(\nu/\nu_0)^\beta$, where κ_0 and β both depend on $\{q, a_{\rm max}, f_s\}$.

For reference, Figure 1 illustrates how opacity properties generally respond to particle properties, for some representative model variations (see Cuzzi et al. 2014, Woitke et al. 2016, or Birnstiel et al. 2018 for more detailed explorations of the parameter-space). When $a_{\rm max} \ll \lambda$, κ_0 is roughly independent of the size cut-off and β is high ($\sim$1.7, as for the small dust grains in the interstellar medium; Finkbeiner et al. 1999). When $a_{\rm max} \gg \lambda$, κ_0 decreases with $a_{\rm max}$ at a rate depending on q (lower q means a steeper fall-off; e.g., Ricci et al. 2010b) and β is lower (scaling roughly with q; Draine 2006). When $a_{\rm max} \sim \lambda$, resonances drive up both κ_0 and β. Porosity dampens those resonant amplifications. Specifically, κ_ν varies with the product $a_{\rm max}f_s$, such that porous particles have a lower κ_0 and higher β than compact particles with the same size distribution (Kataoka et al. 2014).

While continuum luminosities cannot constrain κ_0, information about the particle properties are accessible from the *shape* of an optically thin microwave spectrum, which varies like $L_\nu \propto \kappa_\nu B_\nu(T) \propto \nu^{\alpha_{\rm mm}}$. The spectral index (i.e., the "color") tracks the opacity index, $\alpha_{\rm mm} \approx \alpha_{\rm Pl} + \beta$, where $\alpha_{\rm Pl} \approx 1.7$–$2.0$ approximates the shape of $B_\nu(T)$ for disk-averaged temperatures >15 K. Multiwavelength photometry surveys find $\alpha_{\rm mm} \approx 2$–$3$ (Beckwith & Sargent 1991, Mannings & Emerson 1994, Ricci et al. 2010b,a, 2012), implying a disk-averaged $\beta \leq 1$ and $a_{\rm max} \geq 1$ mm. There is a sort of apocryphal notion that continuum emission traces particles with sizes up to $a_{\rm max} \sim \lambda$. But a more accurate statement is that the emission is most *efficient* with this criterion since it corresponds to the peak κ_0 (giving the most emission per mass), but even much larger particles still contribute. Therein lies the key ambiguity: the opacity can decrease (by orders of magnitude) if larger solids are present (see Fig. 1), and the ambiguities of interpreting β constraints permit such a possibility. Note that the fiducial opacities adopted in the literature ($\sim$1–3 cm^2 g^{-1} at $\lambda = 1.3$ mm) are effectively upper bounds on κ_ν (see Fig. 1), reflecting the fact that $L_{\rm mm}$ measurements are really yielding lower limits on M_s.

Unresolved spectral index measurements naturally gloss over some important complexities. The particle properties, and thereby the opacities, are expected to vary spatially in disks. The (presumably inter-dependent) morphologies of those variations make it difficult to determine the impact of κ_ν changes on inferences of M_s without spatially resolved measurements of $\alpha_{\rm mm}$. Moreover, an unknown fraction of the continuum emission can be optically thick, where $\alpha_{\rm mm} \approx 1.5$–$2.5$ depending on T (or $\alpha_{\rm Pl}$) and the spectral dependence of the albedo (Zhu et al. 2019, Liu 2019). This would diminish unresolved (disk-averaged) estimates of β, again limiting an assessment of the M_s uncertainty due to the opacities.

Shifting attention to the gas mass, there are direct analogues of these same ambiguities. First, there is also the concern that the optically thin approximation is at least partially invalid, particularly for the HD and ^{13}CO lines, implying again that mass may be hidden (M_g is under-estimated). As with the microwave continuum, the emission from an optically thin spectral line traces the produce of temperature and column density (i.e., mass). The key difference is that the line emission originates from a more two-dimensional geometry (radial and vertical), which can potentially incorporate pronounced temperature gradients that are directly related to the distribution of the tracer abundances. This is especially significant for M_g estimates from the HD ground state line, which by a quirk of its excitation physics has an exponential T dependence (Bergin et al. 2013). In any case, a good model or measurement of $T(r, z)$ is required for a robust estimate of M_g (see Section 2.4).

The key ambiguities in M_g measurements from optically thin emission lines come from the uncertain chemical abundances of the tracer molecules relative to H_2. For HD, the associated chemical network is simple enough that the gas phase abundance should be fairly robust; the open questions are related to the unaccounted contribution of enhanced D fractionation in ices or hydrocarbons that could lead to an under-estimate of HD/H_2 (and therefore M_g). The situation with CO is more complicated. Presuming the interstellar CO/H_2 abundance ratio and isotopic fractionation (Frerking et al. 1982), the observed CO isotopologue luminosities from disks suggest surprisingly low M_g values (by a factor of $\sim$5–10; Williams & Best 2014) relative to other gas tracers in the same disks (Chapillon et al. 2010, Favre et al. 2013, Kama et al. 2016) or estimates of M_s and presumed interstellar solids-to-gas ratios ($\zeta \approx 0.01$; Kastner et al. 1997, Dutrey et al. 2003, Ansdell et al. 2016, Long et al. 2017). This apparent anomaly can be reconciled by invoking a higher solids-to-gas ratio ($\zeta \geq 0.1$) or modifying the assumed abundances. The right direction and amplitude of abundance changes are expected from various chemical processes, including adsorption onto solids ("freezeout"; Aikawa et al. 1997, 2002, Dutrey et al. 1997), isotope-selective photodissociation (Visser et al. 2009, Miotello et al. 2014, 2016), or C and O sequestration into other species (e.g., CO_2 ice, complex organics; Reboussin et al. 2015, Yu et al. 2017, Miotello et al. 2017, Bosman et al. 2018, Dodson-Robinson et al. 2018).

As for the continuum emission, additional information about these ambiguities is in principle available from resolved maps of the spatial distribution of the relevant tracers.

2.2. Sizes

The first step toward measuring the spatial mass distributions in disks is an estimate of their sizes. But there is no obvious general definition for size from an observational perspective, since any metric depends on the prescription adopted for interpreting the radial variation of a given tracer. There is an expectation that the mass distribution exhibits a break at some radius, beyond which it drops off more precipitously into the background. That practical notion was originally motivated by the sharp cut-off of larger bodies in the Solar System around 40 au (e.g., Luu & Jewitt 2002), but it is now supported by many disk observations (e.g., Andrews et al. 2018). Nevertheless, there is no *a priori* knowledge of the detailed behavior of that transition, nor how it manifests in different tracers. The ideal solution would be to employ a robust parametric model for the physical structure and use that to homogenize size measurements. But it should be clear at this point in the review that such an effort is littered with ambiguities. Recognizing that ignorance for the time being, the more practical approach is to assign an empirical definition of size as the effective radius

that encircles some fixed fraction of the tracer luminosity.

There are resolved size measurements of the $\lambda \approx 1$ mm continuum emission from solids for >100 nearby disks, with effective radii spanning ∼5–200 au (Tripathi et al. 2017, Tazzari et al. 2017, Barenfeld et al. 2017, Andrews et al. 2018). Crude size constraints, falling in the same range, are available for another ∼100 targets (e.g., Eisner et al. 2018, Cieza et al. 2019). The lower bound of that range is presumably resolution-limited. There is a striking tight correlation between the continuum sizes and luminosities (Andrews et al. 2010, Piétu et al. 2014), with a scaling relation $L \propto R^{1/2}$ (Tripathi et al. 2017, Andrews et al. 2018). Figure 2 shows the continuum size distribution and this size–luminosity scaling. This relationship is presumably produced by the evolution of disk solids (Tripathi et al. 2017, Rosotti et al. 2019), although extracting more information in that context is potentially muddled by a degeneracy with high optical depths (Andrews et al. 2018, Zhu et al. 2019).

The spatial variation of the microwave spectrum shape suggests that the continuum size is correlated with the observing frequency (e.g., Pérez et al. 2012, 2015, Tazzari et al. 2016). The proper context of such inferences will be revisited elsewhere, but explicit estimates of the shapes of this correlation indicate a modest scaling, $R \propto \nu^{0.2-0.5}$ (Tripathi et al. 2018). An alternative size metric is available from the extent of the optical/infrared starlight scattered off the disk surface. Despite the difficulties of measuring that signal at large distances from the star, the current suite of scattered light images clearly indicate that the μm-sized dust grains that reflect starlight are distributed out to considerably large distances than the larger particles responsible for the microwave continuum.

Sensitivity limitations mean there are many fewer size measurements in spectral line tracers of the gas. The ^{12}CO lines typically extend to radii of ∼100–500 au (Ansdell et al. 2018), although there are a few exceptional outliers on the high end (e.g., Guilloteau & Dutrey 1998, Panić et al. 2009). Smaller disks presumably exist, but are missing in current samples due to sensitivity limitations (e.g., Barenfeld et al. 2017). Nevertheless, tracer size comparisons for individual disks make it clear that the spectral line emission extends typically twice as far from the host star as the microwave continuum (Ansdell et al. 2018). Some of that size discrepancy is produced by the different optical depths of the tracers (Hughes et al. 2008, Trapman et al. 2019), but detailed modeling efforts have convincingly argued for a genuine variation between the tracer densities as well (e.g., Panić et al. 2009, Andrews et al. 2012, de Gregorio-Monsalvo et al. 2013, Rosenfeld et al. 2013b, Facchini et al. 2017). The implication is a radial decrease in the solids-to-gas ratio, an expected consequence of the evolution of disk solids that will be addressed further in Section 4.

2.3. Surface Density Profiles

Spatially resolved measurements of the same mass tracers introduced in Section 2.1 can in principle be used to constrain the radial surface density profiles of the solids (Σ_s) or gas (Σ_g), albeit subject to the ambiguities and caveats discussed above.

A key emphasis on the interpretation of modest resolution (∼20–50 au) interferometric observations of the microwave continuum morphologies has been on estimating the density gradient (Guilloteau & Dutrey 1998, Andrews & Williams 2007b, Piétu et al. 2007, Andrews et al. 2009, 2010, Isella et al. 2009, Piétu et al. 2014), since that is presumed to influence the architectures of future planetary systems (e.g., Miguel et al. 2011). The mechanics and parameterizations of the modeling used to measure those gradients varies substantially between studies, but a crude distillation of the results in terms of a broken power-law

profile suggests $\Sigma_s \propto 1/r$ or shallower in the inner disk, and $\Sigma_s \propto 1/r^3$ or steeper at large radii. It is worth remembering that these data are really measuring gradients at large radii: the extrapolations to the inner disk are determined by the functional form of the adopted Σ_s parameterization and at best a few resolution elements that trace a turnover toward the inner disk. The inferred surface density normalizations from these studies typically span $\sim$0.001–1 g cm^{-2} (of solids) at radii of 50–100 au, comparable to the disk-averaged $\langle\Sigma_s\rangle$ expected from the normalization of the continuum size–luminosity relation and similar assumptions about the temperatures and opacities (Tripathi et al. 2017). Efforts to more robustly quantify Σ_s have been stymied by the evidence that optical depths are likely high inside a few tens of au and that κ_ν clearly varies with radius (see Section 4).

2.4. Thermal Structure

physics overview: irradiation heating, dominated by the vertical distribution of small grains. temperature depends on host luminosity/spectrum, particle size, porosity, compositions (IR opacity), optical depths, flaring angle (set partially by turbulence/diffusion), and any shadowing. surface layers can be super-heated and Tgas can deviate from Tdust when line cooling becomes comparable to small grains. secondary heating source could be mechanical work from viscosity in inner disk. smaller effects from radioactivity, CRs (?), see d'alessio papers.

observations: you want to access optically thick tracers over a range of disk locations. some information in infrared SED, limits on vertical distribution of dust (scattering, thermal). there are benchmarks available (in principle) from chemical signatures (e.g., CO snowlines). the ideal approach is to use the excitation constraints from multiple transitions of a given molecular species, and use that to sound out things. limited success in this so far, because its time-consuming. but it really is necessary. worry about non-LTE in some cases. ultimately want to link these things all together. this is the key...once you have a T(r,z) model that is robust to the data, then you can try to get gas densities.

2.5. Dynamical Structure

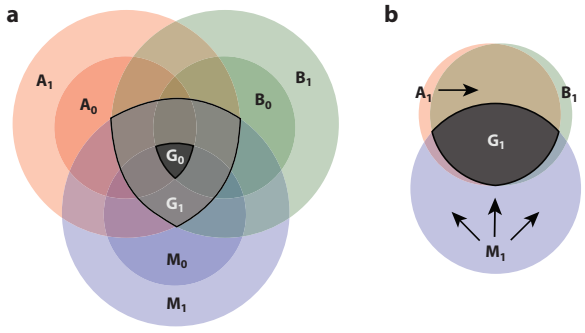

Figure 2

Figure caption with descriptions of parts a and b

Summary

TBD

3. DEMOGRAPHIC INSIGHTS

3.1. Links to Host Masses

3.2. Environmental Effects

two key environmental effects, on local scales/"internal" (multiplicity) and global scales/"external" (stripping via tidal encounters or harsh irradiation from nearby massive stars).

3.2.1. Multiplicity. basic mechanics of disk truncation idea. field population multiplicity rates and separation/eccentricity distributions. differences there for nearby low-mass clusters. that implies an expectation that multiplicity is pretty important in shaping observables. see evidence for diminished continuum luminosities for pairs with closer separations (projected). weird CB disk exception. primaries have more mass in majority, but not all, cases. population of stars in multiples follows similar scaling with host mass. there is not good evidence for a continuum size vs separation relationship predicted by theory; maybe partly due to not using gas as the tracer, but could also be related to evidence for non-coplanarity (discuss that). worth noting that fainter disks at smaller separations does not necessarily imply lower densities (consider how much emission you would get for v small optically thick disks). FIGURE: show separation-Lmm distribution for all available pairs (maybe in left panel of 2-panel figure).

3.2.2. Close Encounters. need to read up

3.2.3. External Photoevaporation. need to catch up. FIGURE: probably second panel here showing Lmm versus distance from theta1 Oric.

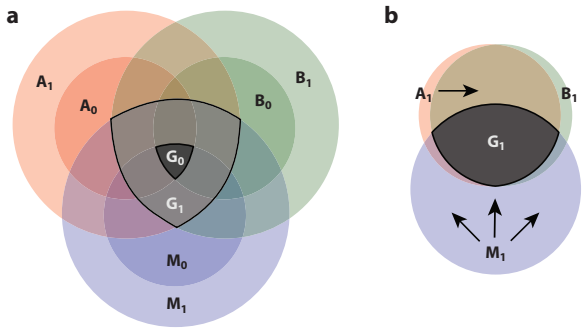

Figure 3

Figure caption with descriptions of parts a and b

Table 1 Table caption

Head 1 (units)[a]	Head 2	Head 3	Head 4	Head 5 (units)
Column 1	Column 2	Column3[b]	Column4	Column
Column 1	Column 2	Column3	Column4	Column
Column 1	Column 2	Column3	Column4	Column
Column 1	Column 2	Column3	Column4	Column

[a]Table footnote; [b]second table footnote.

1. List entry number 1,
2. List entry number 2,
3. List entry number 3,

4. List entry number 4, and
5. List entry number 5.

Term A: definition
Term B: definition
Term C: defintion

Here is an example of a extract.

This is an example text of quote or extract. This is an example text of quote or extract.

SIDEBARS

Sidebar text goes here.

Sidebar Second-Level Heading

More text goes here.

Sidebar third-level heading. Text goes here.

$$a = b \text{ ((Single Equation Numbered))} \tag{1}$$

Equations can also be multiple lines as shown in Equations 2 and 3.

$$c = 0 \text{ ((Multiple Lines, Numbered))} \tag{2}$$

$$ac = 0 \text{ ((Multiple Lines, Numbered))} \tag{3}$$

SUMMARY POINTS

1. Summary point 1. These should be full sentences.
2. Summary point 2. These should be full sentences.
3. Summary point 3. These should be full sentences.
4. Summary point 4. These should be full sentences.

FUTURE ISSUES

1. Future issue 1. These should be full sentences.
2. Future issue 2. These should be full sentences.
3. Future issue 3. These should be full sentences.
4. Future issue 4. These should be full sentences.

DISCLOSURE STATEMENT

If the authors have noting to disclose, the following statement will be used: The authors are not aware of any affiliations, memberships, funding, or financial holdings that might be perceived as affecting the objectivity of this review.

ACKNOWLEDGMENTS

Acknowledgements, general annotations, funding.

LITERATURE CITED

Please see the Style Guide document for instructions on preparing your Literature Cited.

The citations should be listed in alphabetical order, with no titles. For example:

```
\begin{thebibliography}{00}

\bibitem[Acevedo \& Fitzjarrald(2001)]{Acevedo:01}
Acevedo O, Fitzjarrald D. 2001.
\textit{J. Atmos. Sci.} 58:2650--67

\bibitem[Acevedo et~al.(2009)Acevedo, Moraes, Degrazia, Fitzjarrald, Manzi \&
  Campos]{Acevedo:09}
\textit{Agric. For. Meteorol.} 149:1--10

\bibitem[Baas et~al.(2006)Baas, Steeneveld, {van de Weil} \& Holtslag]{Baas:09}
Baas P, Steeneveld G, {van de Weil} B, Holtslag A. 2006.
\textit{J. Atmos. Sci.} 63:3045--54

\bibitem[Badran et~al.(1991)]{Badran:91}
Badran F, Thiria S, Crepon M. 1991.
\textit{J. Geophys. Res.} 96:20,521--29

\bibitem[Bakas \& Ioannou(2007)]{Bakas:07}
Bakas NA, Ioannou PJ. 2007.
\textit{J. Atmos. Sci.} 64:1509--29

\bibitem[Calanca et~al.(1998)]{Calanca:98}
Calanca P, Forrer J, Rotach M. 1998.
\textit{Q. J. R. Meteorol. Soc.} 124:1--18

\bibitem[D'Asaro \& Lien(2000)]{DAsaro:00}
D'Asaro EA, Lien RC. 2000.
\textit{J. Phys. Oceanog.} 30:123--45

\bibitem[de~Silva et~al.(1996)de~Silva, Fernando, Eaton \& Hebert]{deSilva:96}
de~Silva I, Fernando H, Eaton F, Hebert D. 1996.
\textit{Earth Planetary Sci. Let.} 143:217--31



\end{thebibliography}
```

LITERATURE CITED

Aikawa, Y., Umebayashi, T., Nakano, T., & Miyama, S. M. 1997, , 486, L51, 10.1086/310837

Aikawa, Y., van Zadelhoff, G. J., van Dishoeck, E. F., & Herbst, E. 2002, , 386, 622, 10.1051/0004-6361:20020037

Alibert, Y., Mordasini, C., Benz, W., & Winisdoerffer, C. 2005, , 434, 343, 10.1051/0004-6361:20042032

Andre, P., & Montmerle, T. 1994, , 420, 837, 10.1086/173608

Andrews, S. M. 2015, , 127, 961, 10.1086/683178

Andrews, S. M., Czekala, I., Wilner, D. J., et al. 2010, , 710, 462, 10.1088/0004-637X/710/1/462

Andrews, S. M., Rosenfeld, K. A., Kraus, A. L., & Wilner, D. J. 2013, , 771, 129, 10.1088/0004-637X/771/2/129

Andrews, S. M., & Williams, J. P. 2005, , 631, 1134, 10.1086/432712

—. 2007a, , 671, 1800, 10.1086/522885

—. 2007b, , 659, 705, 10.1086/511741

Andrews, S. M., Wilner, D. J., Hughes, A. M., Qi, C., & Dullemond, C. P. 2009, , 700, 1502, 10.1088/0004-637X/700/2/1502

Andrews, S. M., Wilner, D. J., Hughes, A. M., et al. 2012, , 744, 162, 10.1088/0004-637X/744/2/162

Andrews, S. M., Wilner, D. J., Zhu, Z., et al. 2018, , 820, L40, 10.3847/2041-8205/820/2/L40

Ansdell, M., Williams, J. P., van der Marel, N., et al. 2016, , 828, 46, 10.3847/0004-637X/828/1/46

Ansdell, M., Williams, J. P., Trapman, L., et al. 2018, , 859, 21, 10.3847/1538-4357/aab890

Barenfeld, S. A., Carpenter, J. M., Sargent, A. I., Isella, A., & Ricci, L. 2017, , 851, 85, 10.3847/1538-4357/aa989d

Beckwith, S. V. W., & Sargent, A. I. 1991, , 381, 250, 10.1086/170646

—. 1993, , 402, 280, 10.1086/172131

Beckwith, S. V. W., Sargent, A. I., Chini, R. S., & Guesten, R. 1990, , 99, 924, 10.1086/115385

Bergin, E. A., Cleeves, L. I., Gorti, U., et al. 2013, , 493, 644, 10.1038/nature11805

Birnstiel, T., Ormel, C. W., & Dullemond, C. P. 2011, , 525, A11, 10.1051/0004-6361/201015228

Birnstiel, T., Dullemond, C. P., Zhu, Z., et al. 2018, , 869, L45, 10.3847/2041-8213/aaf743

Bosman, A. D., Walsh, C., & van Dishoeck, E. F. 2018, , 618, A182, 10.1051/0004-6361/201833497

Cassen, P., & Moosman, A. 1981, Icarus, 48, 353, 10.1016/0019-1035(81)90051-8

Chapillon, E., Parise, B., Guilloteau, S., Dutrey, A., & Wakelam, V. 2010, , 520, A61, 10.1051/0004-6361/201014841

Chiang, E., & Laughlin, G. 2013, , 431, 3444, 10.1093/mnras/stt424

Cieza, L. A., Ruíz-Rodríguez, D., Hales, A., et al. 2019, , 482, 698, 10.1093/mnras/sty2653

Cuzzi, J. N., Estrada, P. R., & Davis, S. S. 2014, , 210, 21, 10.1088/0067-0049/210/2/21

D'Alessio, P., Calvet, N., & Hartmann, L. 2001, , 553, 321, 10.1086/320655

Dartois, E., Dutrey, A., & Guilloteau, S. 2003, , 399, 773, 10.1051/0004-6361:20021638

de Gregorio-Monsalvo, I., Ménard, F., Dent, W., et al. 2013, , 557, A133, 10.1051/0004-6361/201321603

Debes, J. H., Jang-Condell, H., Weinberger, A. J., Roberge, A., & Schneider, G. 2013, , 771, 45, 10.1088/0004-637X/771/1/45

Debes, J. H., Weinberger, A. J., & Schneider, G. 2008, , 673, L191, 10.1086/527546

Dodson-Robinson, S. E., Evans, II, N. J., Ramos, A., Yu, M., & Willacy, K. 2018, , 868, L37, 10.3847/2041-8213/aaf0fd

Dohnanyi, J. S. 1969, , 74, 2531, 10.1029/JB074i010p02531

Draine, B. T. 2006, , 636, 1114, 10.1086/498130

Dressing, C. D., & Charbonneau, D. 2013, , 767, 95, 10.1088/0004-637X/767/1/95

Dutrey, A., Guilloteau, S., & Guelin, M. 1997, , 317, L55

Dutrey, A., Guilloteau, S., & Simon, M. 2003, , 402, 1003, 10.1051/0004-6361:20030317

Eisner, J. A., Arce, H. G., Ballering, N. P., et al. 2018, , 860, 77, 10.3847/1538-4357/aac3e2

Facchini, S., Birnstiel, T., Bruderer, S., & van Dishoeck, E. F. 2017, , 605, A16, 10.1051/0004-

6361/201630329
Favre, C., Cleeves, L. I., Bergin, E. A., Qi, C., & Blake, G. A. 2013, , 776, L38, 10.1088/2041-8205/776/2/L38
Finkbeiner, D. P., Davis, M., & Schlegel, D. J. 1999, , 524, 867, 10.1086/307852
Flaherty, K. M., Hughes, A. M., Rosenfeld, K. A., et al. 2015, , 813, 99, 10.1088/0004-637X/813/2/99
Frerking, M. A., Langer, W. D., & Wilson, R. W. 1982, , 262, 590, 10.1086/160451
Garufi, A., Meeus, G., Benisty, M., et al. 2017, , 603, A21, 10.1051/0004-6361/201630320
Guilloteau, S., & Dutrey, A. 1998, , 339, 467
Guilloteau, S., Dutrey, A., Wakelam, V., et al. 2012, , 548, A70, 10.1051/0004-6361/201220331
Hayashi, C. 1981, Progress of Theoretical Physics Supplement, 70, 35, 10.1143/PTPS.70.35
Henning, T., & Stognienko, R. 1996, , 311, 291
Howard, A. W., Marcy, G. W., Johnson, J. A., et al. 2010, Science, 330, 653, 10.1126/science.1194854
Hughes, A. M., Wilner, D. J., Andrews, S. M., Qi, C., & Hogerheijde, M. R. 2011, , 727, 85, 10.1088/0004-637X/727/2/85
Hughes, A. M., Wilner, D. J., Qi, C., & Hogerheijde, M. R. 2008, , 678, 1119, 10.1086/586730
Ida, S., & Lin, D. N. C. 2004, , 604, 388, 10.1086/381724
Isella, A., Carpenter, J. M., & Sargent, A. I. 2009, , 701, 260, 10.1088/0004-637X/701/1/260
Kama, M., Bruderer, S., Carney, M., et al. 2016, , 588, A108, 10.1051/0004-6361/201526791
Kastner, J. H., Zuckerman, B., Weintraub, D. A., & Forveille, T. 1997, Science, 277, 67, 10.1126/science.277.5322.67
Kataoka, A., Okuzumi, S., Tanaka, H., & Nomura, H. 2014, , 568, A42, 10.1051/0004-6361/201323199
Kataoka, A., Tanaka, H., Okuzumi, S., & Wada, K. 2013, , 554, A4, 10.1051/0004-6361/201321325
Koerner, D. W., Sargent, A. I., & Beckwith, S. V. W. 1993, Icarus, 106, 2, 10.1006/icar.1993.1154
Kusaka, T., Nakano, T., & Hayashi, C. 1970, Progress of Theoretical Physics, 44, 1580, 10.1143/PTP.44.1580
Liu, H. B. 2019, arXiv e-prints. 1904.00333
Long, F., Herczeg, G. J., Pascucci, I., et al. 2017, , 844, 99, 10.3847/1538-4357/aa78fc
Luu, J. X., & Jewitt, D. C. 2002, , 40, 63, 10.1146/annurev.astro.40.060401.093818
Mannings, V., & Emerson, J. P. 1994, , 267, 361
Marsh, K. A., & Mahoney, M. J. 1992, , 395, L115, 10.1086/186501
McClure, M. K., Bergin, E. A., Cleeves, L. I., et al. 2016, , 831, 167, 10.3847/0004-637X/831/2/167
Miguel, Y., Guilera, O. M., & Brunini, A. 2011, , 412, 2113, 10.1111/j.1365-2966.2010.17887.x
Min, M., Canovas, H., Mulders, G. D., & Keller, C. U. 2012, , 537, A75, 10.1051/0004-6361/201117333
Min, M., Rab, C., Woitke, P., Dominik, C., & Ménard, F. 2016, , 585, A13, 10.1051/0004-6361/201526048
Miotello, A., Bruderer, S., & van Dishoeck, E. F. 2014, , 572, A96, 10.1051/0004-6361/201424712
Miotello, A., van Dishoeck, E. F., Kama, M., & Bruderer, S. 2016, , 594, A85, 10.1051/0004-6361/201628159
Miotello, A., van Dishoeck, E. F., Williams, J. P., et al. 2017, , 599, A113, 10.1051/0004-6361/201629556
Miyake, K., & Nakagawa, Y. 1993, Icarus, 106, 20, 10.1006/icar.1993.1156
Molyarova, T., Akimkin, V., Semenov, D., et al. 2017, , 849, 130, 10.3847/1538-4357/aa9227
Osterloh, M., & Beckwith, S. V. W. 1995, , 439, 288, 10.1086/175172
Panić, O., Hogerheijde, M. R., Wilner, D., & Qi, C. 2009, , 501, 269, 10.1051/0004-6361/200911883
Pérez, L. M., Isella, A., Carpenter, J. M., & Chandler, C. J. 2015, , 783, L13, 10.1088/2041-8205/783/1/L13
Pérez, L. M., Carpenter, J. M., Chandler, C. J., et al. 2012, , 760, L17, 10.1088/2041-

8205/760/1/L17
Piétu, V., Dutrey, A., & Guilloteau, S. 2007, , 467, 163, 10.1051/0004-6361:20066537
Piétu, V., Guilloteau, S., Di Folco, E., Dutrey, A., & Boehler, Y. 2014, , 564, A95, 10.1051/0004-6361/201322388
Pollack, J. B., Hollenbach, D., Beckwith, S., et al. 1994, , 421, 615, 10.1086/173677
Reboussin, L., Wakelam, V., Guilloteau, S., Hersant, F., & Dutrey, A. 2015, , 579, A82, 10.1051/0004-6361/201525885
Ricci, L., Testi, L., Natta, A., & Brooks, K. J. 2010a, , 521, A66, 10.1051/0004-6361/201015039
Ricci, L., Testi, L., Natta, A., et al. 2010b, , 512, A15, 10.1051/0004-6361/200913403
Ricci, L., Trotta, F., Testi, L., et al. 2012, , 540, A6, 10.1051/0004-6361/201118296
Rosenfeld, K. A., Andrews, S. M., Hughes, A. M., Wilner, D. J., & Qi, C. 2013a, , 774, 16, 10.1088/0004-637X/774/1/16
Rosenfeld, K. A., Andrews, S. M., Wilner, D. J., Kastner, J. H., & McClure, M. K. 2013b, , 775, 136, 10.1088/0004-637X/775/2/136
Rosotti, G. P., Booth, R. A., Tazzari, M., et al. 2019, arXiv e-prints. 1905.00021
Simon, M., Dutrey, A., & Guilloteau, S. 2000, , 545, 1034, 10.1086/317838
Stolker, T., Dominik, C., Min, M., et al. 2016, , 596, A70, 10.1051/0004-6361/201629098
Tanaka, H., Inaba, S., & Nakazawa, K. 1996, , 123, 450, 10.1006/icar.1996.0170
Tazzari, M., Testi, L., Ercolano, B., et al. 2016, , 588, A53, 10.1051/0004-6361/201527423
Tazzari, M., Testi, L., Natta, A., et al. 2017, ArXiv e-prints. 1707.01499
Terebey, S., Shu, F. H., & Cassen, P. 1984, , 286, 529, 10.1086/162628
Trapman, L., Facchini, S., Hogerheijde, M. R., van Dishoeck, E. F., & Bruderer, S. 2019, arXiv e-prints. 1903.06190
Trapman, L., Miotello, A., Kama, M., van Dishoeck, E. F., & Bruderer, S. 2017, , 605, A69, 10.1051/0004-6361/201630308
Tripathi, A., Andrews, S. M., Birnstiel, T., & Wilner, D. J. 2017, , 845, 44, 10.3847/1538-4357/aa7c62
Tripathi, A., Andrews, S. M., Birnstiel, T., et al. 2018, , 861, 64, 10.3847/1538-4357/aac5d6
Visser, R., van Dishoeck, E. F., & Black, J. H. 2009, , 503, 323, 10.1051/0004-6361/200912129
Weidenschilling, S. J. 1977, , 180, 57
Weintraub, D. A., Sandell, G., & Duncan, W. D. 1989, , 340, L69, 10.1086/185441
Williams, J. P., & Best, W. M. J. 2014, , 788, 59, 10.1088/0004-637X/788/1/59
Woitke, P., Min, M., Pinte, C., et al. 2016, , 586, A103, 10.1051/0004-6361/201526538
Yu, M., Evans, II, N. J., Dodson-Robinson, S. E., Willacy, K., & Turner, N. J. 2017, , 841, 39, 10.3847/1538-4357/aa6e4c
Zhu, Z., Zhang, S., Jiang, Y.-F., et al. 2019, arXiv e-prints. 1904.02127